ELSEVIER

Physica B 314 (2002) 145–149

PHYSICA B

www.elsevier.com/locate/physb

Nonequilibrium band structure of nano-devices

S. Hackenbuchner[a,*], M. Sabathil[a], J.A. Majewski[a], G. Zandler[a], P. Vogl[a], E. Beham[a], A. Zrenner[a], P. Lugli[b]

[a] *Walter Schottky Institute and Physics Department, Technical University of Munich, Am Coulombwall, D-85748 Garching, Germany*
[b] *Department of Electronic Engineering, University of Rome Tor Vergata, 00133 Roma, Italy*

Abstract

A method is developed for calculating, in a consistent manner, the realistic electronic structure of three-dimensional (3-D) heterostructure quantum devices under bias and its current density close to equilibrium. The nonequilibrium electronic structure is characterized by local Fermi levels that are calculated self-consistently. We have applied this scheme to predict asymmetric Stark shifts and tunneling of confined electrons and holes in single-dot GaAs/InGaAs photodiodes. © 2002 Elsevier Science B.V. All rights reserved.

PACS: 73.63.Kv; 78.67.Hc; 79.60.Jv

Keywords: Nano-devices; Simulations; Quantum dots; Stark shift

1. Introduction

A realistic simulator of three-dimensional (3-D) semiconductor nano-structures and optoelectronic nano-devices should meet two requirements. Firstly, it should model the electronic structure of any combination of quantum wells, wires, and dots accurately on a length scale from nm to μm. Secondly, a device simulator should self-consistently account for the charge redistribution under applied voltage and for the resulting current (see, e.g., [1]). Recently, several methods have been published that can realistically predict the equilibrium electronic structure of 3-D nano-structures. They are based on one-band [2], or several-band k.p models [3–5], tight binding methods [6] or pseudopotential techniques [7,8]. Some of them include free and bound charge distributions self-consistently [2,3]. Most quantum transport methods that include the electronic structure beyond a one-band description are still limited to one spatial dimension [9–11]. Thus, a simultaneous realistic treatment of the electronic structure and the quantum transport problem for 3-D structures still poses a challenging task.

In this paper, we present first results on a simulator that we have developed for a wide class of 3-D Si and III–V nano-structures that meets both requirements mentioned above, albeit via a WKB-type approach for the current only valid close to equilibrium, where the concept of local quasi-Fermi levels is still justifiable. We have applied this approach to study self-assembled GaAs/InAs single-quantum-dot photodiodes [12] and predict a hole tunneling rate that greatly

*Corresponding author. Tel.: +49-89-289-12762; fax: +49-89-289-12737.

E-mail address: hackenbuchner@wsi.tum.de (S. Hackenbuchner).

0921-4526/02/$ - see front matter © 2002 Elsevier Science B.V. All rights reserved.
PII: S0921-4526(01)01345-X

exceeds the electrons' one in lens-shaped quantum dots.

2. Three-dimensional nano-device simulator

The simulator solves the 8-band-k.p-Schrödinger–Poisson equation for arbitrarily shaped 3-D heterostructure device geometries, and for any (III–V and Si/Ge) combination of materials and alloys. It includes band offsets of the minimal and higher band edges, absolute deformation potentials [13], local density exchange and correlations (i.e. the Kohn–Sham equations), total elastic strain energy [14,15], long-range Hartree potential induced by charged impurity distributions, voltage induced charge redistributions, piezo- and pyroelectric charges, as well as surface charges, in a fully self-consistent manner. The charge density is calculated for a given applied voltage by assuming the carriers to be in a local equilibrium characterized by energy-band dependent local quasi-Fermi levels $E_{Fc}(\mathbf{x})$ for charge carriers of type c (i.e. in the simplest case, one for holes and one for electrons),

$$n_c(\mathbf{x}) = \sum_i |\Psi_{ic}(\mathbf{x})|^2 f\left(\frac{E_{Fc}(\mathbf{x}) - E_{ic}}{k_B T}\right). \qquad (1)$$

These local quasi-Fermi levels are determined by global current conservation $\nabla \bullet \mathbf{j}_c = 0$, where the current is assumed to be proportional to the density and to the gradient of the quasi-Fermi level (associated with each band) exactly as in the semiclassical limit (see, e.g. [16]). The carrier wave functions Ψ_{ic} and energies E_{ic} are calculated by solving the multi-band Schrödinger–Poisson equation. The open system is mimicked by using mixed Dirichlet and von Neumann boundary conditions [10,17,18] at Ohmic contacts. The charge density at these contacts is assumed to be equal to the bulk equilibrium density. Thus, the quasi-Fermi levels and the potential in the contact region are fixed according to the applied voltage. Our method leads to globally orthogonal eigenstates including valence (split-off, light and heavy hole) and conduction band states. Further, it automatically includes tunneling, and yields optical transition energies and as well as optical matrix elements.

According to Eq. (1), one and the same bound state $\Psi_{ic}(\mathbf{x})$ may get occupied differently at different positions according to the spatial dependence of $E_{Fc}(\mathbf{x})$. This is a consequence of invoking the well-defined but semiclassical concept of local Fermi levels together with nonlocal quantum mechanics. Fortunately, no conflict arises for situations close to equilibrium since the spatial variation of the occupancy of any given eigenstate turns out to be negligible for 3 reasons: (i) Deeply bound states do not contribute to the current and thus do not lead to a gradient of the Fermi level; (ii) the Fermi level has the largest variation in regions where the density is very low (within barriers, for example); (iii) very extended states that are treated formally as bound states in our method are either not occupied because of their high energy, or occur in regions of high density (near contacts, for example) where the quasi-Fermi level is nearly constant.

The computational methods, that will be described elsewhere, solve the Kohn–Sham–Schrödinger, Poisson and current continuity equations iteratively using conjugate gradient, inverse-iteration, Jacobi–Davidson [19] and predictor–corrector methods [20] in an inhomogeneous finite difference framework.

3. Application: single dot spectroscopy

We have applied our simulator to study theoretically single-quantum-dot photodiodes [12,21–23]. We consider self-assembled InGaAs quantum dots with a diameter of 30–40 nm and heights of 4–8 nm that are embedded in the intrinsic region of an n-i-Schottky diode (see inset of Fig. 2 for a schematic cross section). Such dots with a nominal In concentration of only 50% and correspondingly high exciton energies close to 1.3 eV have been fabricated recently [12]. Both experiments of [12] as well as earlier ones by the Skolnick group [21] have shown asymmetric Stark shifts and associated dipoles that indicate inverted electron–hole alignments with the electron at the base and the hole at the top of the dot, in contrast to what earlier theoretical calculations [4,5,15] had predicted.

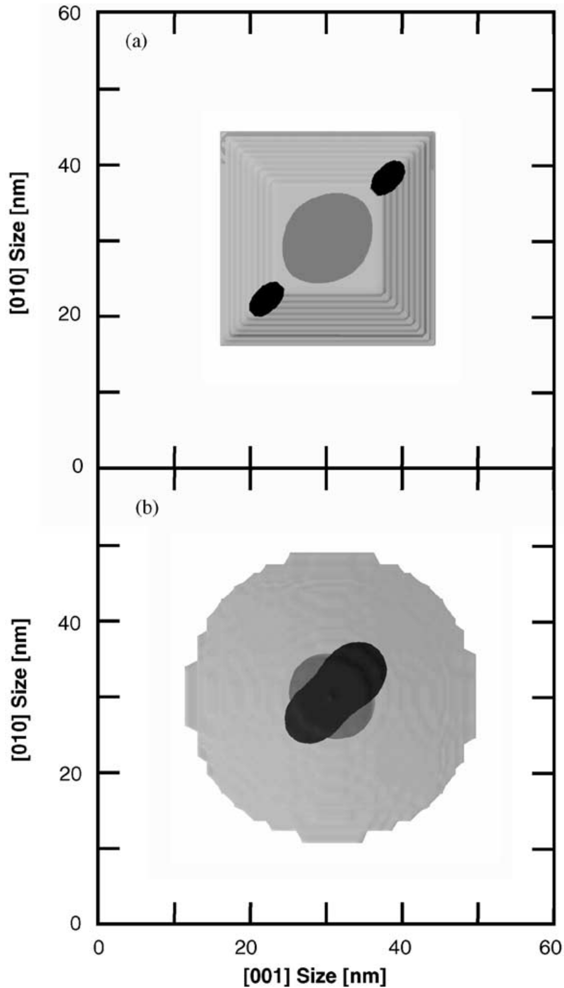

Fig. 1. Top view of some theoretically analyzed InGaAs dot shapes. The height in the center is 8 nm for both dot shapes (a) and (b). The black dots indicate the calculated density of the hole ground state and the dark gray areas the electron ground state, respectively. The isosurfaces represent 50% of the maximum charge density.

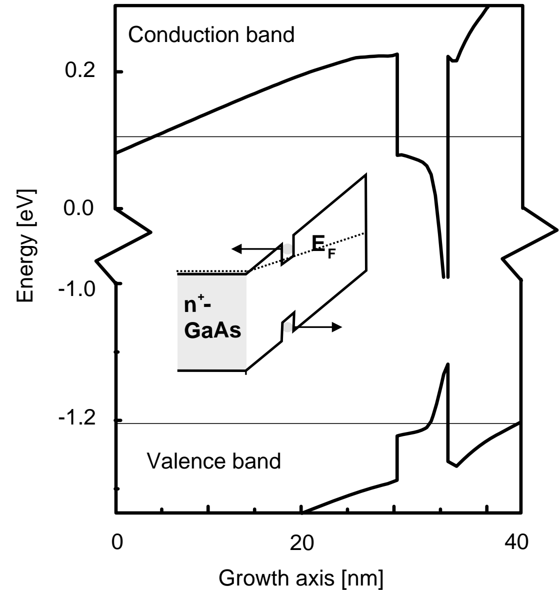

Fig. 2. Band edge profile through the center of lens-shaped InGaAs quantum dot of height 6 nm, diameter 40 nm, and alloy profile as shown in the inset of Fig. 3. The thin lines indicate the electron and hole ground state energy, respectively. The inset shows a schematic diagram of the single-dot photodiode under negative bias with the calculated electron quasi-Fermi level E_{Fn}.

We have examined several dot sizes, shapes, and alloy profiles as a function of applied bias in the strain-relaxed structures in a sufficiently large region surrounding the dot, including the wetting layer. We find, in agreement with [3], dots of pyramidal shape to possess large piezoelectric polarization charges in the corners that lead to a strong hole confinement near the dot edges (Fig. 1a). By contrast, lens-shaped dots of similar size are found to lead to electron *and* hole states near the center of the lens which significantly improves the exciton absorption (Fig. 1b). In the following discussion, we focus on lens-shaped dots with a height and average alloy composition that leads to a zero bias exciton energy of ~ 1.3 eV as in the experiments of [12]. Fig. 2 shows the conduction and valence band edge profile in the intrinsic region cutting through the center of a dot with an alloy concentration of 16% at the base and 44% at the top and a Gaussian profile (see Fig. 3). The electron ground state is seen to be significantly less localized than the hole state. Most importantly, we find the hole to be localized at the apex (top) and the electron at the base exactly as has been suggested by [21]. These results are a consequence of the pronounced band bending (that may be considered as an effective built-in field as can be deduced from Fig. 2) that is caused by the large composition variation within the dot. This result remains valid also for higher in concentrations. We

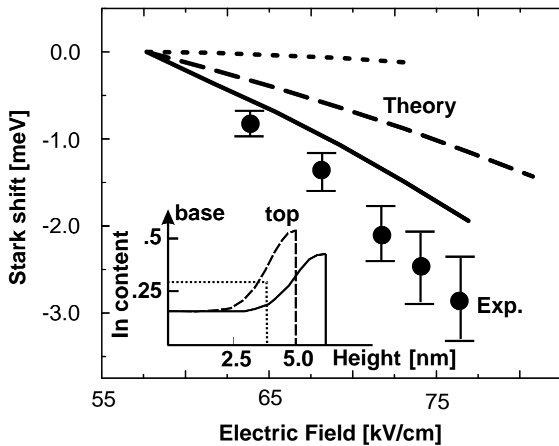

Fig. 3. Calculated shift of the exciton ground state as a function of the electric field for 3 different lens-shaped dots with alloy profiles near the dot center as indicated in the inset. The dots are experimental results from [12].

emphasize that the strain-induced piezoelectric charges are small in the presently studied dots and do not contribute to this unusual inversion of electron and hole localization. Since the hole state is pinned to the band edge near the top of the dot, its energy follows the same linear trend as a function of applied bias as the band edge. This leads to an almost linear Stark shift of the ground state exciton as a function of the electric field, as shown in Fig. 3 for different alloy profiles and dot heights. The gradient of these curves is seen to decrease for dots with smaller height and flatter alloy profiles. The comparison with experiment [12] in Fig. 3 shows that the measured data can only be explained by assuming a very steep alloy profile. Steep alloy profiles in GaAs/InAs dots have recently been observed experimentally [24].

The inverted localization of the electrons at the base and holes at the top of the dot has interesting consequences for the tunneling of the carriers and the onset of the photocurrent. By calculating the complex band structure [18] and modeling the dot by a quantum well of equal strain, alloy profile and height, we have calculated the resonance energy width (see [25] for a discussion) for a dot structure of 6 nm height and alloy concentration between 16% and 44%. We predict the hole tunneling rate to be 2–4 orders of magnitudes higher than the electron one, in the range of electric fields between 60 and 90 kV/cm. This effect is caused by the fact that the barrier width for the holes is smaller than for the electrons (cf. Fig. 2). We note that the situation is reversed if we assume a hypothetic pseudomorphic rather than a fully relaxed strain. In conclusion, we have shown that the presently developed 3-D device simulator can successfully explain recently found anomalies in asymmetric Stark shifts of InAs/GaAs quantum dots in terms of steep alloy profiles.

Acknowledgements

Financial support by the Deutsche Forschungsgemeinschaft and by the Office of Naval Research under Contract No. N00014-01-1-0242 is gratefully acknowledged.

References

[1] G.W. Zobrist (Ed.), Proceedings of the Seventh International Workshop on Computational Electronics, Glasgow, Scotland, May 22–25, 2000, VLSI Design 10 (2000) 1.

[2] A. Kumar, S.E. Laux, F. Stern, Phys. Rev. B 42 (1990) 5166;
S.E. Laux, in: J.J.H. Miller (Ed.), Proceedings of the Fifth International Conference on Numerical Analysis of Semiconductor Devices and Integrated Circuits (NASECODE V), Boole, Dun Laoghaire, Ireland, 1987, pp. 270–275.

[3] M. Grundmann, O. Stier, D. Bimberg, Phys. Rev. B 59 (1999) 5688.

[4] C. Pryor, Phys. Rev. B 57 (1998) 7190;
C. Pryor, Phys. Rev. B 60 (1999) 2869.

[5] M.A. Cusack, P.R. Briddon, M. Jaros, Phys. Rev. B 54 (1996) R2300.

[6] A. Di Carlo, Proceedings of the 12th International Conference on Nonequilibrium Carrier Dynamics in Semiconductors, Santa Fe, 2001, see this volume.

[7] L.W. Wang, A. Zunger, Phys. Rev. B 59 (1999) 15806.

[8] F. Chirico, A. Di Carlo, P. Lugli, Phys. Rev. B 64 (2001) 045314.

[9] R. Lake, G. Klimeck, R.C. Bowen, D. Jovanovic, J. Appl. Phys 81 (1997) 7845 (project "NEMO"), http://www.cfdrc.com/nemo/index.html.

[10] M.V. Fischetti, Phys. Rev. B 59 (1999) 4901.

[11] D.K. Ferry, R. Akis, D. Vasileska, Electron Device Meeting, IEDM 2000 Technical Digest Papers, pp. 287–290.

[12] F. Findeis, M. Baier, E. Beham, A. Zrenner, G. Abstreiter, Appl. Phys. Lett. 78 (2001) 2958.
[13] C. Van de Walle, Phys. Rev. B 39 (1989) 1871.
[14] C. Pryor, J. Kim, L.W. Wang, A.J. Williamson, A. Zunger, J. Appl. Phys. 83 (2548) 1998.
[15] M. Grundmann, O. Stier, D. Bimberg, Phys. Rev. B 52 (1995) 11969.
[16] S. Selberherr, Analysis and Simulation of Semiconductor Devices, Springer, Wien, 1984.
[17] C.S. Lent, D.J. Kirkner, J. Appl. Phys. 67 (1990) 6353.
[18] W.R. Frensley, Superlattices and Microstructures 11 (1992) 347.
[19] Z. Bai, J. Demmel, J. Dongarra, A. Ruhe, H. van der Vorst (Eds.), Templates for the Solution of Algebraic Eigenvalue Problems, SIAM, Philadelphia, 2000.
[20] A. Trellakis, A.T. Galick, A. Pacelli, U. Ravaioli, J. Appl. Phys. 81 (1997) 7880.
[21] P.W. Fry, I.E. Itskevich, D.J. Mowbray, et al., Phys. Rev. Lett. 84 (2000) 733.
[22] I.E. Itskevich, S.I. Rybchenko, I.I. Tartakovskii, et al., in: N. Miura, T. Ando (Eds.), Proceedings of the 25th International Conference Physics and Semiconductor, Osaka, 2000, p. 1135.
[23] C.M.A. Kapteyn, M. Lion, R. Heitz, et al., Phys. Stat. Sol. (b) 224 (2001) 57.
[24] I. Kegel, T.H. Metzger, A. Lorke, et al., Phys. Rev. B 63 (2001) 035318.
[25] D. M.-T. Kuo, Y.-C. Chang, Phys. Rev. B 61 (2000) 11051.